Chemical Science

ROYAL SOCIETY OF CHEMISTRY

EDGE ARTICLE

View Article Online
View Journal | View Issue

Cite this: *Chem. Sci.*, 2024, **15**, 16096

All publication charges for this article have been paid for by the Royal Society of Chemistry

Spirobifluorene-based hole-transporting materials for RGB OLEDs with high efficiency and low efficiency roll-off†

Qian Li, Yusong Guo, Jingbo Lan, * Yudong Yang, Di Wu * and Zhengyang Bin *

Received 26th July 2024
Accepted 3rd September 2024

DOI: 10.1039/d4sc04979a

rsc.li/chemical-science

In this work, we designed and synthesized three spirobifluorene (SBF)-based hole-transporting materials (HTMs) by incorporating the di-4-tolylamino group at different positions of the SBF skeleton. These materials demonstrate excellent thermal stability with thermal decomposition temperatures (T_d) up to 506 °C and outstanding morphological stability with a glass transition temperature (T_g) exceeding 145 °C. The *meta*-linkage mode between the conjugated skeleton and functional groups in the molecular structure results in electronic decoupling, giving these 3,6-substituted SBFs higher triplet energies (E_T) compared to 2,7-substituted SBFs. This makes the 3,6-substituted SBFs suitable as universal HTMs for red, green, and blue (RGB) organic light emitting diodes (OLEDs). Among the three HTMs, 3,3′,6,6′-tetra(*N*,*N*-ditolylamino)-9,9′-spirobifluorene (**3,3′,6,6′-TDTA-SBF**) exhibits the best device performance, achieving maximum external quantum efficiencies (EQE_{max}) of 26.1%, 26.4%, and 25.4% for RGB phosphorescent OLEDs, with extremely low efficiency roll-off in both green and blue devices. Utilizing **3,3′,6,6′-TDTA-SBF** as the HTM, we have also fabricated narrowband blue OLEDs based on the widely used multiple resonance emitter BCz-BN, which exhibits a EQE_{max} of 29.8% and low efficiency roll-off.

Introduction

Hole-transporting materials (HTMs) play an important role in organic light emitting diode (OLED) devices because of their hole transportation and electron blocking ability in the interfacial region between the hole-transporting layer (HTL) and the light-emitting layer.[1–6] In general, HTMs need to possess high hole mobility, good morphological stability, and an appropriate highest occupied molecular orbital (HOMO) level to ensure a low energy barrier for hole injection to the emitting layer and a suitable lowest unoccupied molecular orbital (LUMO) level to block electron injection from the emitting layer to the HTL.[2,7–11] Triarylamine derivatives are the most widely used HTMs due to their excellent optoelectronic properties.[12–18] Among them, 1,1-bis(4-*N*,*N*-ditolylaminophenyl)cyclohexane (TAPC) is one of the most classical HTMs, owing to its high hole mobility (μ_h), high transparency for visible light, and high triplet energies (E_T) (2.9 eV) for blocking triplet excitons. However, TAPC exhibits a low glass transition temperature (T_g) of 74 °C, lacking proper morphological stability.[19,20]

The 9,9′-spirobifluorene (SBF) structure possesses excellent thermal stability with high decomposition temperature (T_d), high T_g, high E_T, and well-matched frontier molecular orbital (FMO) energy levels with adjacent layers.[21–23] Therefore, SBF-based organic optoelectronic materials have been widely applied in the field of organic light-emitting diodes (OLEDs), perovskite solar cells, and organic lasers.[24–29] In recent years, SBF-based HTMs have also been extensively explored.[1,2,30–33] The C2 and C7 positions of SBF have the highest electrophilic reactivity.[34] As a result, a considerable amount of research on HTMs is focused on C2 and C7-substituted SBF derivatives.[30–33,35–38] However, the C2 and C7-substitutions have been noted to reduce the E_T of SBF derivatives due to the electronic coupling between electron-donating groups at C2 and/or C7-positions and the biphenyl of fluorene *via* a *para*-linkage mode.[31,39] For example, the introduction of arylamines at the C2 and C7 positions results in E_T values of 2.31 and 2.29 eV for the compounds, compared to 2.88 eV for SBF.[31,39]

In this work, we design and synthesize a series of C3 and C6-substituted SBF derivatives containing two or four di-4-tolylamino groups, respectively, including 3,3′,6,6′-tetra(*N*,*N*-ditolylamino)-9,9′-spirobifluorene (**3,3′,6,6′-TDTA-SBF**), 3,3′-di(*N*,*N*-ditolylamino)-9,9′-spirobifluorene (**3,3′-DDTA-SBF**), and 3,6-di(*N*,*N*-ditolylamino)-9,9′-spirobifluorene (**3,6-DDTA-SBF**) (Scheme 1). These SBF-based triarylamine derivatives present

Key Laboratory of Green Chemistry and Technology of Ministry of Education College of Chemistry, Sichuan University, 29 Wangjiang Road, Chengdu 610064, People's Republic of China. E-mail: binzhengyang@scu.edu.cn; woody@scu.edu.cn; jingbolan@scu.edu.cn

† Electronic supplementary information (ESI) available: Experimental details, crystallographic data, and photophysical and thermal performances of the compounds. CCDC 2370368 (**3,6-DDTA-SBF**). For ESI and crystallographic data in CIF or other electronic format see DOI: https://doi.org/10.1039/d4sc04979a

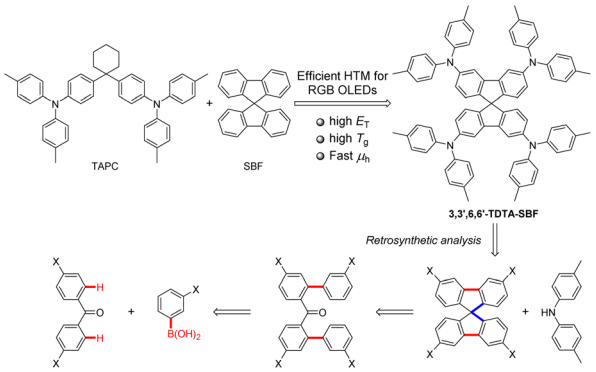

Scheme 1 Molecular design concept and retrosynthetic analysis.

high E_T and wide HOMO/LUMO differences owing to the electronic decoupling between electron-donating di-4-tolylamino groups at C3 and/or C6-positions and the biphenyl of fluorene *via* a *meta*-linkage mode, and are therefore suitable as HTMs for red, green, and blue (RGB) OLEDs. Moreover, SBF endows these HTMs with good thermal stability and excellent hole-transporting properties, beneficial for the assembly of high-performance OLEDs.

Results and discussion

Synthesis and characterization

Chelation-assisted transition metal-catalyzed *ortho*-C–H arylation has emerged as a powerful method to accomplish aryl–aryl coupling.[40–46] Retrosynthetic analysis indicates that **3,3′,6,6′-TDTA-SBF** can be prepared through a Buchwald–Hartwig amination of 3,3′,6,6′-tetrahalogenated SBF with di-*p*-tolylamine (Scheme 1). 3,3′,6,6′-Tetrahalogenated SBF can be synthesized by chelation-assisted transition metal-catalyzed *ortho*-C–H diarylation of 4,4′-dihalogenated benzophenone, followed by an intramolecular Friedel–Crafts spiroannulation reaction (Scheme 1). Therefore, *ortho*-C–H diarylation was initially explored by a model reaction of benzophenone with phenylboronic acid under palladium catalysis. However, the diarylated product was not observed under the Pd-catalyzed conditions. Fortunately, when employing benzophenone *O*-methyl oxime and phenylboronic acid pinacol ester as substrates, the diarylated product **3a** could be obtained in a yield of 53% (Table S1,† entry 1). Further optimization of reaction conditions was carried out. Finally, **3a** was afforded in 71% yield in the presence of 10 mol% of $Pd(dba)_2$, 20 mol% of *N*-acetyl-L-phenylalanine as a ligand, and 1.5 equiv. of Ag_2CO_3 as an oxidant in 1,1,1,3,3,3-hexafluoro-2-propanol (HFIP) solvent at 100 °C for 36 h under a nitrogen atmosphere (Table S1,† entry 4).

Adopting optimized reaction conditions, the chelation-assisted Pd-catalyzed *ortho*-C–H diarylation of bis(4-chlorophenyl)methanone *O*-methyl oxime (**1b**) with *meta*-methoxyphenylboronic acid pinacol ester produced **3b** in 62% yield (Scheme 2). Then, methane sulfonic acid (MsOH)-promoted intramolecular Friedel–Crafts alkylation provided the key 3,3′,6,6′-tetrasubsitituted SBF intermediate **4** in 82% yield. The yield of side reactions occurring at the *ortho*-position

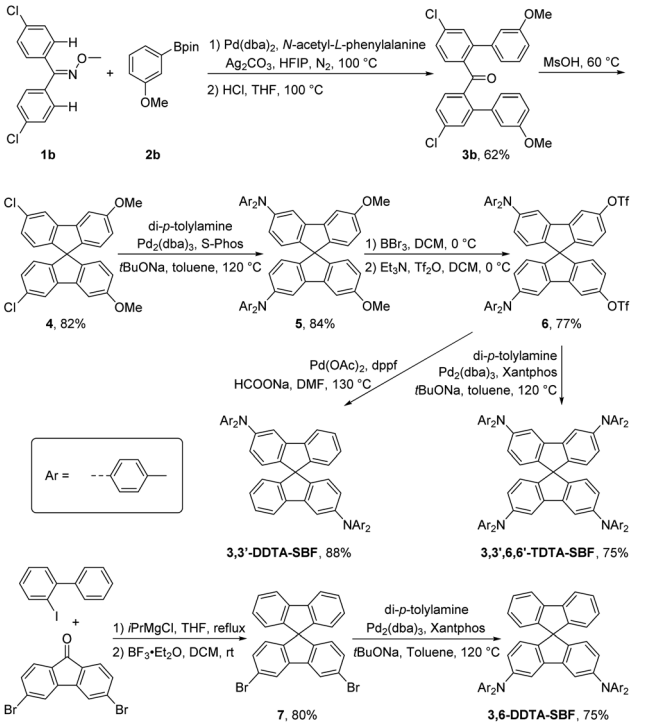

Scheme 2 Synthesis of 3,3′,6,6′-TDTA-SBF, 3,3′-DDTA-SBF and 3,6-DDTA-SBF.

of the methoxy group is very low. The Buchwald–Hartwig amination of **4** with di-*p*-tolylamine gave **5** in 84% yield. **5** underwent a deprotection of methyl ether in the presence of BBr_3 and then an esterification reaction using trifluoromethanesulfonic anhydride (Tf_2O) to deliver **6** in 77% yield. Buchwald–Hartwig amination was once again performed to produce **3,3′,6,6′-TDTA-SBF** in 75% yield. The triflate group was reductively removed from the SBF core of **6** catalyzed by palladium, yielding **3,3′-DDTA-SBF** in 88% yield. Subsequently, **3,6-dibromo-SBF** was prepared through the nucleophilic addition of 3,6-dibromo-9*H*-fluoren-9-one by using 2-iodo-1,1′-biphenyl in the presence of ^{i}PrMgCl and a subsequent intramolecular Friedel–Crafts alkylation reaction, which underwent a Buchwald–Hartwig amination to afford **3,6-DDTA-SBF** (Scheme 2). The structures of the three compounds were confirmed by ^{1}H NMR, ^{13}C NMR and high-resolution mass spectrometry (HRMS). The structure of **3,6-DDTA-SBF** was further confirmed by its single crystal X-ray data. In the single crystal X-ray structure, **3,6-DDTA-SBF** molecules mainly adopt an edge-to-face packing mode *via* multiple intermolecular C–H···π interaction networks, accompanied by a weak π···π interaction with 3.69 Å between the two benzene rings of the intermolecular di-4-tolylamino group (Fig. S1†). Unfortunately, attempts to acquire single crystals of **3,3′,6,6′-TDTA-SBF** were unsuccessful as a result of its low crystallinity.

Theoretical calculations

Density functional theory (DFT) and time-dependent DFT (TD-DFT) calculations were performed at the B3LYP/6-31G(d) level (Fig. 1). **3,3′,6,6′-TDTA-SBF** is essentially composed of four

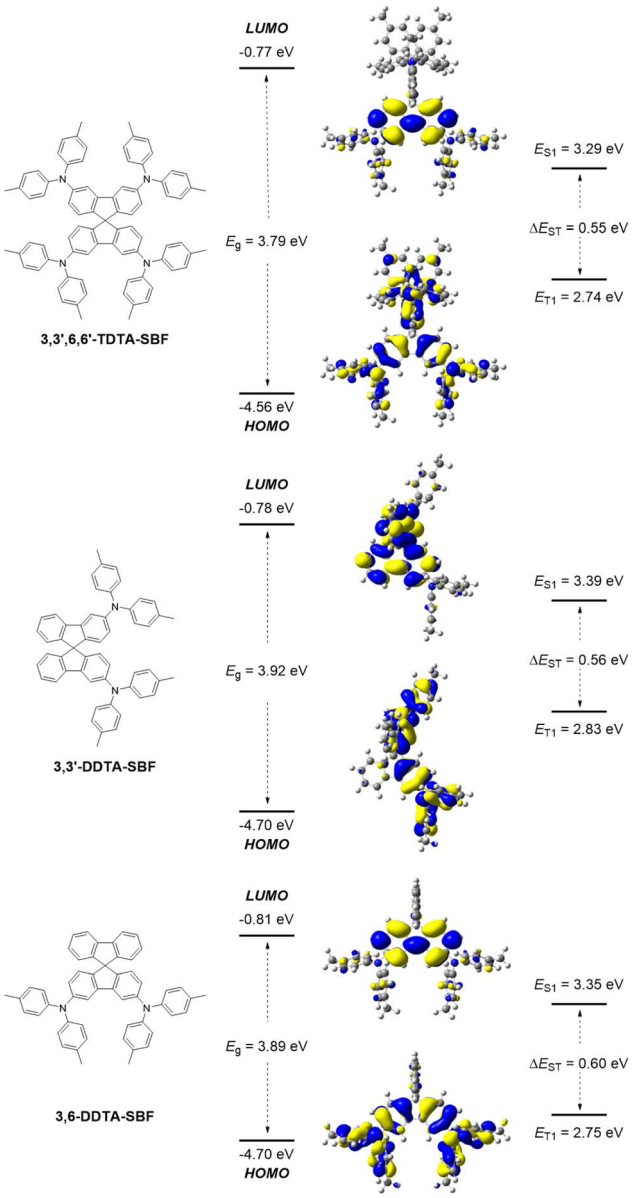

Fig. 1 Frontier orbital distributions and energy level alignments of 3,3′,6,6′-TDTA-SBF, 3,3′-DDTA-SBF and 3,6-DDTA-SBF.

triarylamines through the connections of two Csp^2–Csp^2 σ-bonds and a quaternary carbon core. Therefore, its HOMO is distributed on all twelve benzene rings and four nitrogen atoms of the four triarylamines due to the highly symmetrical characteristics, while its LUMO is mainly focused on one of the two fluorene units. Similarly, the HOMO of **3,3′-DDTA-SBF** is distributed on two triphenylamines, while its LUMO is extended to the two fluorene units of the SBF core. The HOMO of **3,6-DDTA-SBF** is also distributed on two triphenylamines, and its LUMO is mainly localized on the fluorene substituted by the di-4-tolylamino group. Calculation results indicate that the three compounds possess similar HOMO energy levels of −4.56 eV for **3,3′,6,6′-TDTA-SBF**, −4.70 eV for **3,3′-DDTA-SBF** and −4.70 eV for **3,6-DDTA-SBF**, while the LUMO energy levels were calculated to be −0.77, −0.78 and −0.81 eV for **3,3′,6,6′-TDTA-SBF**, **3,3′-DDTA-SBF** and **3,6-DDTA-SBF**, respectively. Accordingly, these compounds all exhibit large energy gaps (E_g) of about 3.9 eV. Moreover, the E_{T1} value was calculated to be 2.74 eV for **3,3′,6,6′-TDTA-SBF**, 2.83 eV for **3,3′-DDTA-SBF** and 2.75 eV for **3,6-DDTA-SBF**. The high E_{T1} is a key property to prevent leakage of triplet excitons from the emitting layer to the HTL, especially for the blue emitting OLED.

Electronic and physical properties

The photophysical properties of these SBF-based triarylamine derivatives were studied. The strong absorption peaks at 310–313 nm correspond to π–π* transitions, which represent the characteristic absorption of the SBF scaffold (Fig. 2a and Table 1). The weak absorption bands at 350–400 nm may be attributed to n–π* transitions (Fig. 2a). The optical band gaps (E_g) of **3,3′,6,6′-TDTA-SBF**, **3,3′-DDTA-SBF** and **3,6-DDTA-SBF** were calculated from the onset of their absorption spectra to be 3.07 eV, 3.12 eV and 3.09 eV, respectively (Table 1). Their maximum emission wavelengths are at 401–402 nm (Fig. 2b and Table 1). Despite having different numbers of diarylamino

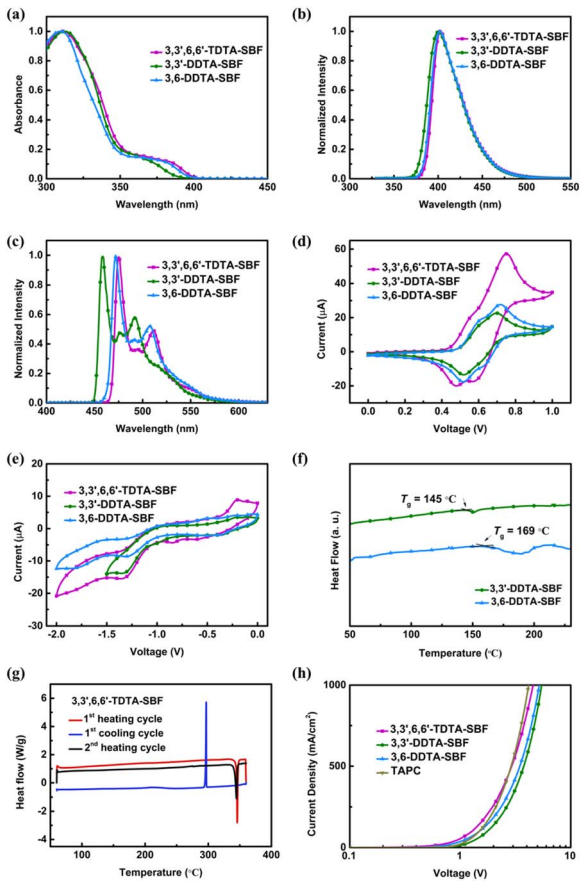

Fig. 2 (a) UV-vis absorption spectra, (b) emission spectra at 298 K, (c) phosphorescence spectra at 77 K in toluene, and cyclic voltammetry (CV) data (d) in oxidation and (e) in reduction: CH_2Cl_2/[NBu_4PF_6] 0.1 M of 3,3′,6,6′-TDTA-SBF, 3,3′-DDTA-SBF and 3,6-DDTA-SBF. (f) DSC curves of 3,3′-DDTA-SBF and 3,6-DDTA-SBF. (g) DSC curves of 3,3′,6,6′-TDTA-SBF. (h) The current density–voltage (J–V) curves using 3,3′,6,6′-TDTA-SBF-, 3,3′-DDTA-SBF-, 3,6-DDTA-SBF- and TAPC-based hole-only devices (HODs).

Table 1 Electronic and physical properties

Property	3,3′,6,6′-TDTA-SBF	3,3′-DDTA-SBF	3,6-DDTA-SBF
λ_{abs} [a] [nm]	311	313	310
λ_{em} [a] [nm]	402	401	401
E_g [b] [eV]	3.07	3.12	3.09
E_{T1} [c] [eV]	2.66	2.75	2.68
T_g [°C]	—	145	169
T_d [°C]	506	430	413
HOMO [d] [eV]	−5.20	−5.19	−5.20
LUMO [d] [eV]	−3.08	−3.16	−3.07
μ_h [e] [$cm^2 V^{-1} S^{-1}$]	3.83×10^{-2}	1.61×10^{-2}	2.53×10^{-2}

[a] Measured in toluene solution (1.0×10^{-5} M), where λ_{abs} is the absorption peak and λ_{em} is the photoluminescence peak at room temperature. [b] Calculated from the onset of the absorption spectra. [c] Calculated from the first phosphorescence peak at 77 K in toluene. [d] Calculated from CV curves with ferrocene as the internal standard using the formulae $E_{HOMO} = -[E_{ox} - E_{(Fc/Fc+)} + 4.8]$ eV and $E_{LUMO} = -[E_{red} - E_{(Fc/Fc+)} + 4.8]$ eV. [e] Hole mobility (μ_h). TAPC: $\mu_h = 3.84 \times 10^{-2}$ $cm^2 V^{-1} s^{-1}$.

substituents and different substituted sites, the absorption and emission spectra of the three compounds are almost identical, probably owing to the electronic decoupling of the *meta*-connection mode in both the ground and excited states. The phosphorescence emission spectra measured at 77 K in toluene provide the corresponding E_{T1} of 2.66 eV, 2.75 eV and 2.68 eV for **3,3′,6,6′-TDTA-SBF**, **3,3′-DDTA-SBF** and **3,6-DDTA-SBF**, respectively (Fig. 2c and Table 1).

Electrochemical investigations were performed by cyclic voltammetry (CV) in CH_2Cl_2 solution (Fig. 2d and e). The HOMO levels were measured at −5.20 eV for **3,3′,6,6′-TDTA-SBF**, −5.19 eV for **3,3′-DDTA-SBF** and −5.20 eV for **3,6-DDTA-SBF** (Table 1). These values provide advantages for hole injection into the emitting layer. Additionally, the LUMO levels were measured at −3.08 eV for **3,3′,6,6′-TDTA-SBF**, −3.16 eV for **3,3′-DDTA-SBF** and −3.07 eV for **3,6-DDTA-SBF** (Table 1). The shallow LUMO level would help to prevent electrons from escaping the emission layer. Subsequently, their T_d were detected by thermogravimetric analysis (TGA) at a rate of 10 °C min^{-1} under a nitrogen atmosphere, and the T_g was measured by differential scanning calorimetry (DSC) under a nitrogen atmosphere (Fig. 2f and g). Benefiting from the rigid and orthogonal conjugated skeleton of the SBF core, these compounds exhibit excellent thermal stabilities with a very high T_d of 506 °C, 430 °C and 413 °C for **3,3′,6,6′-TDTA-SBF**, **3,3′-DDTA-SBF** and **3,6-DDTA-SBF**, respectively (Table 1). The DSC measurement, performed in the temperature range from 50 °C to 260 °C, demonstrates that **3,3′-DDTA-SBF** and **3,6-DDTA-SBF** possess high T_g, which is 145 °C and 169 °C, respectively (Table 1). However, the T_d of **3,3′,6,6′-TDTA-SBF** was not observed to be in this temperature range. Therefore, the DSC measurement of **3,3′,6,6′-TDTA-SBF** was subsequently performed in a larger temperature range from 50 °C to 360 °C. The experimental result indicates that **3,3′,6,6′-TDTA-SBF** melts at 346 °C. As shown in Fig. 2f, before the sample completely melts, a rather smooth DSC curve is observed without any clue of glass transition or other phase transformation, demonstrating excellent morphological stability.

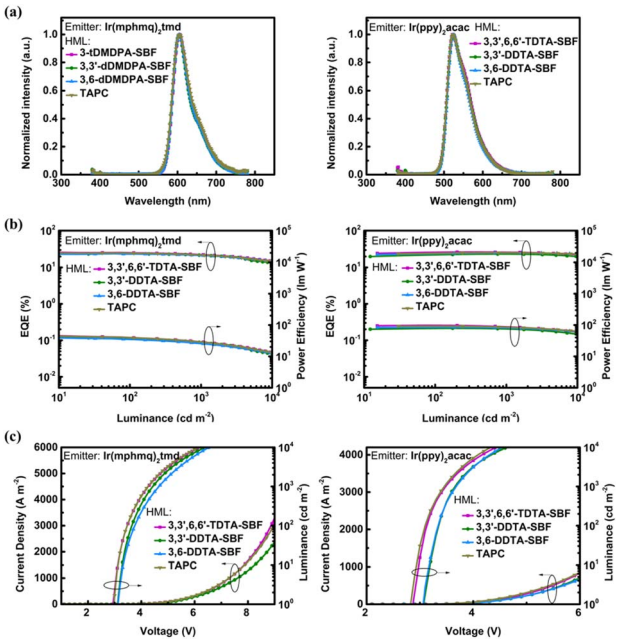

Fig. 3 OLED device performances. (a) Electroluminescence spectra at a luminance of 1000 cd m^{-2}, (b) luminance and current density *versus* voltage curves, and (c) EQE and power efficiency *versus* luminance curves of red (left) and green (right) PhOLED devices.

Subsequently, the hole transport properties of these SBF-based triarylamine derivatives were investigated. A hole-only device (HOD) was fabricated according to the device architecture of ITO/HAT-CN (10 nm)/HTM (120 nm)/HAT-CN (10 nm)/Al (100 nm), which was employed as both the hole injection and electron-blocking layer. The HOD of TAPC was also fabricated for comparison. We use the space-charge-limited current (SCLC) method to calculate the μ_h values (Fig. S3†). All three compounds exhibit excellent hole-transporting properties, with μ_h values of 3.83×10^{-2} $cm^2 V^{-1} s^{-1}$, 1.61×10^{-2} $cm^2 V^{-1} s^{-1}$ and 2.53×10^{-2} $cm^2 V^{-1} s^{-1}$ for **3,3′,6,6′-TDTA-SBF**, **3,3′-DDTA-SBF** and **3,6-DDTA-SBF**, respectively (Fig. 3). These values are comparable to that of TAPC (3.84×10^{-2} $cm^2 V^{-1} s^{-1}$, Fig. 2h), which is well-known for its excellent hole-transporting properties in OLED HTMs.

Electroluminescence performances

The device performance of **3,3′,6,6′-TDTA-SBF**, **3,3′-DDTA-SBF** and **3,6-DDTA-SBF** as HTMs was further investigated in phosphorescent OLEDs (PhOLEDs). The performances are summarized in Fig. 3, S4, S5† and Tables 2, S1.† The optimized HTM thickness is 30 nm (Fig. S5 and Table S3†). First, bis[4-methyl-2-(3,5-dimethylphenyl)quinoline]tetramethyl heptadionate iridium(III) ($Ir(mphmq)_2(tmd)$) was selected as a red phosphor and 4,4′-bis(9*H*-carbazol-9-yl)biphenyl (CBP) as a host. The optimized red PhOLED device structure was ITO/HAT-CN (10 nm)/HTM (25 nm)/TCTA (10 nm)/CBP: 1 wt% $Ir(mphmq)_2tmd$ (10 nm)/TmPyPB (50 nm)/LiF (0.8 nm)/Al (100 nm). In these devices, HAT-CN and LiF were used as the hole injection and electron injection materials, respectively, 4,4′,4″-tris(9*H*-carbazol-9-yl) triphenylamine (TCTA) as an exciton-blocking material, and

Table 2 Summary of OLED performance

Emitter	HTM	EL_{peak} [nm]	V_{on}[a] [V]	CIE[b] [x, y]	EQE_{max}/1000/5000[c] [%]	PE_{max}/1000/5000[d] [lm W^{-1}]
$Ir(mphmq)_2tmd$	**3,3′,6,6′-TDTA-SBF**	605	3.1	[0.63, 0.36]	26.1/22.3/17.8	46.3/28.6/18.1
	3,3′-DDTA-SBF	605	3.2	[0.63, 0.37]	23.9/21.7/15.5	41.5/28.0/15.7
	3,6-DDTA-SBF	605	3.3	[0.63, 0.37]	24.0/21.1/17.1	39.2/25.2/16.5
	TAPC	605	3.1	[0.63, 0.37]	25.1/22.1/17.0	44.9/28.1/17.6
$Ir(ppy)_2acac$	**3,3′,6,6′-TDTA-SBF**	524	3.0	[0.32, 0.63]	26.4/26.0/24.3	97.6/87.1/71.4
	3,3′-DDTA-SBF	525	3.2	[0.32, 0.63]	23.2/23.2/21.6	78.6/74.2/61.0
	3,6-DDTA-SBF	525	3.2	[0.32, 0.64]	25.0/25.0/24.3	85.2/80.4/68.9
	TAPC	523	3.0	[0.32, 0.63]	25.4/25.3/24.3	92.6/84.8/71.3
Flrpic	**3,3′,6,6′-TDTA-SBF**	471	3.1	[0.16, 0.36]	25.4/21.4/19.8	52.6/31.4/24.6
	3,3′-DDTA-SBF	473	3.3	[0.16, 0.37]	23.9/21.0/18.6	48.0/31.1/23.4
	3,6-DDTA-SBF	472	3.3	[0.16, 0.38]	25.0/21.8/18.1	51.1/31.5/21.6
	TAPC	474	3.1	[0.16, 0.37]	24.8/20.0/17.5	51.5/30.3/22.5
BCz-BN	**3,3′,6,6′-TDTA-SBF**	487	3.0	[0.10, 0.35]	29.8/24.0/19.2	53.4/29.6/19.7
	3,3′-DDTA-SBF	486	3.2	[0.11, 0.35]	24.9/20.5/16.8	42.0/23.8/16.0
	3,6-DDTA-SBF	486	3.2	[0.11, 0.34]	25.7/20.9/17.0	42.3/23.9/16.0
	TAPC	487	3.1	[0.10, 0.36]	28.7/20.9/17.2	50.5/25.4/17.4

[a] Turn-on voltage. [b] Commission Internationale de l'Eclairage (CIE). [c] Maximum external quantum efficiency and external quantum efficiencies at a luminance of 1000 cd m^{-2} and 5000 cd m^{-2}. [d] Maximum power efficiency and power efficiencies at a luminance of 1000 cd m^{-2} and 5000 cd m^{-2}.

1,3,5-tri(*m*-pyrid-3-ylphenyl)benzene (TmPyPB) as an electron-transporting material (ETM). The molecular structure and the corresponding PhOLED device structure are shown in Fig. S4.† The devices which employed **3,3′,6,6′-TDTA-SBF**, **3,3′-DDTA-SBF** and **3,6-DDTA-SBF** as HTMs exhibit excellent performances with maximum external quantum efficiencies (EQE_{max}) of 26.1%, 24.0% and 23.9%, respectively, as well as low efficiency roll-off (Fig. 3 and Table 2). Under the same device fabricating conditions, the PhOLED based on TAPC as the HTM exhibits a relatively lower device efficiency with an EQE_{max} of 25.1% than that of **3,3′,6,6′-TDTA-SBF**.

The green PhOLED devices were fabricated employing bis(2-phenylpyridine)iridium(III)-acetylacetonate ($Ir(ppy)_2(acac)$) as a green phosphor and CBP as the host material. Using HAT-CN as a hole injection layer led to a lower device efficiency, and therefore, the optimized green PhOLED device structure was ITO/HTM (30 nm)/TCTA (10 nm)/CBP: 10 wt% $Ir(ppy)_2acac$ (20 nm)/TmPyPB (40 nm)/LiF (0.8 nm)/Al (100 nm) (Fig. S4†). **3,3′,6,6′-TDTA-SBF**, **3,3′-DDTA-SBF** and **3,6-DDTA-SBF** all show excellent performance as the HTMs of green PhOLEDs with an EQE_{max} of 26.4%, 25.0% and 23.2%, respectively (Fig. 3 and Table 2). Notably, **3,3′,6,6′-TDTA-SBF** as a hole transport layer exhibits extremely low device efficiency roll-off, and the EQE at 1000 cd m^{-2} maintained 98% of its peak value. For comparison, the PhOLED device using TAPC instead of **3,3′,6,6′-TDTA-SBF** as the hole transport layer was fabricated under identical conditions, which shows a relatively lower EQE_{max} of 25.4%.

The existing SBF-based triarylamine derivatives have rarely been used as HTMs for blue PhOLED devices due to their low E_T. A hole HTM with an E_T value is crucial for blue PhOLEDs, as it prevents triplet energy from transferring back from the blue emitter to the neighboring hole-transporting layer.[47–50] The SBF-based triarylamine derivatives herein developed possess high triplet energy levels with E_{T1} from 2.66 eV to 2.75 eV. Therefore, the blue PhOLED devices were fabricated employing bis(3,5-difluoro-2-(2-pyridyl)phenyl)-2-carboxypyridyl iridium(III) (FIrpic) as a blue phosphor, 3,3′-di(9*H*-carbazol-9-yl)-1,1′-biphenyl (mCBP) as the host material, and **3,3′,6,6′-TDTA-SBF**, **3,3′-DDTA-SBF** or **3,6-DDTA-SBF** as the HTM, respectively. The blue PhOLED device using TAPC as the HTM was also fabricated as a comparison. The optimized blue PhOLED device structure was ITO/HTM (30 nm)/TCTA (10 nm)/mCBP: 15 wt% Flrpic (23 nm)/TmPyPB (40 nm)/LiF (0.8 nm)/Al (100 nm) (Fig. S4†). Among all four tested HTMs, including TAPC, the blue PhOLED device using **3,3′,6,6′-TDTA-SBF** as the HTM exhibits the best performance with an EQE_{max} of 25.4% and low efficiency roll-off

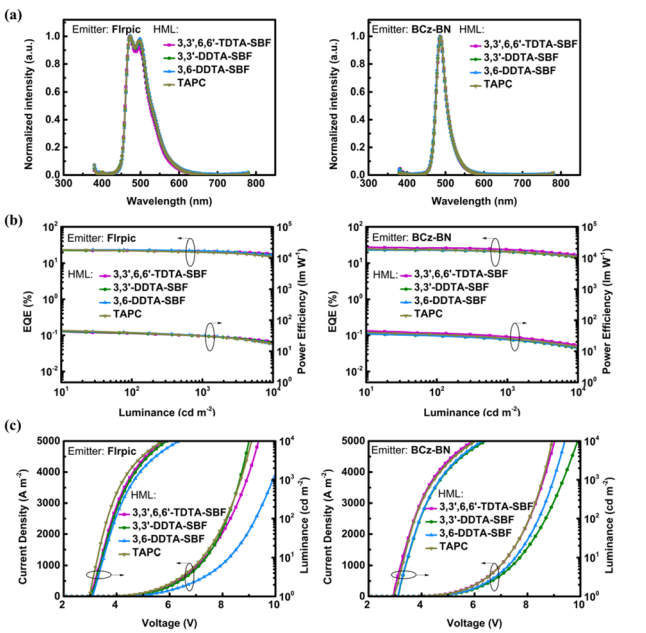

Fig. 4 OLED device performances. (a) Electroluminescence spectra at a luminance of 1000 cd m^{-2}, (b) luminance and current density *versus* voltage curves, and (c) EQE and power efficiency *versus* luminance curves of blue PhOLED (left) devices and narrowband-emitting BN-MR OLED (right) devices.

(Fig. 4 and Table 2). At luminance levels of 1000 cd m^{-2} and 5000 cd m^{-2}, the device efficiencies are well-preserved at 21.4% and 19.8%, respectively.

In recent years, boron–nitrogen-based multiple resonance (BN-MR) emitters have shown great potential for application in the next generation of wide-colour gamut OLED displays with ultrahigh resolution (UHD) due to their exceptionally narrowband emissions. Among these, BCz-BN is one of the most classical BN-MR emitters. In order to explore the extensive possibility of these SBF-based triarylamine derivatives as HTMs, we fabricated OLED devices based on BCz-BN as the emitter, mCBP as the host, Flrpic as the sensitizer, and **3,3′,6,6′-TDTA-SBF**, **3,3′-DDTA-SBF** and **3,6-DDTA-SBF** as the HTMs, respectively. An OLED device using TAPC as the HTM was also fabricated for comparison. The optimized BN-MR emitter-based OLED device structure was ITO/HML (30 nm)/TCTA (10 nm)/mCBP: 15 wt% Flrpic: 0.5 wt% BCz-BN (23 nm)/TmPyPB (40 nm)/LiF (0.8 nm)/Al (100 nm) (Fig. S4†). The OLED device using **3,3′,6,6′-TDTA-SBF** as the HTL achieves an EQE_{max} of 29.8% and low efficiency roll-off (Fig. 4 and Table 2), revealing the great potential of these molecules as universal HTMs for the assembly of blue OLEDs.

Conclusions

In summary, we have developed a highly efficient palladium catalyst system to conduct the diarylation of benzophenone *O*-methyl oxime derivatives, which provides convenience for the development of 3,3′,6,6′-tetrasubstituted SBF derivatives. Based on this rapid and concise synthetic strategy, **3,3′,6,6′-TDTA-SBF** and **3,3′-DDTA-SBF** were successfully obtained. For comparison, **3,6-DDTA-SBF** is prepared by a classical route. Further investigation on electronic and physical properties as well as electroluminescence performances indicates that **3,3′,6,6′-TDTA-SBF** not only possesses high E_T and T_g values but also fast μ_h, enabling the assembly of high-performance RGB PhOLEDs with an EQE_{max} of 26.1%, 26.4%, and 25.4%, respectively, as well as narrowband blue OLEDs with an EQE_{max} of 29.8%. This work not only introduces a universal HTM based on the 3,6-substituted SBF skeleton for assembling high-performance RGB OLEDs but also highlights the effectiveness of the C–H activation method in discovering high-performance organic functional materials.

Data availability

Data are available in the article and ESI.†

Author contributions

Q. Li carried out most parts of the experiments. Y. Guo performed some of the synthesis. J. Lan designed and directed the project. J. Lan, D. Wu, Y. Yang and Z. Bin wrote and modified the manuscript. All authors contributed to discussions.

Conflicts of interest

There are no conflicts to declare.

Acknowledgements

We acknowledge financial support from the National Key R&D Program of China (No. 2021YFA1500100), National Natural Science Foundation of China (No. 22371196, 22071162, 22171188, and 22275127), Natural Science Foundation of Sichuan, China (2022NSFSC0029), and Fundamental Research Funds for the Central Universities. We are also thankful for the support of associate researcher Shaolan Wang from the Analytical and Testing Center of Sichuan University and Comprehensive Training Platform Specialized Laboratory, College of Chemistry, Sichuan University.

Notes and references

1 S. Jhulki and J. N. Moorthy, *J. Mater. Chem. C*, 2018, **6**, 8280–8325.
2 Shahnawaz, S. S. Swayamprabha, M. R. Nagar, R. A. K. Yadav, S. Gull, D. K. Dubey and J.-H. Jou, *J. Mater. Chem. C*, 2019, **7**, 7144–7158.
3 Q. Huang, G. A. Evmenenko, P. Dutta, P. Lee, N. R. Armstrong and T. J. Marks, *J. Am. Chem. Soc.*, 2005, **127**, 10227–10242.
4 S. Chen, J. Wei, K. Wang, C. Wang, D. Chen, Y. Liu and Y. Wang, *J. Mater. Chem. C*, 2013, **1**, 6594–6602.
5 H. Je, S. Cho, N. Y. Kwon, D. W. Lee, M. J. Cho and D. H. Choi, *ACS Appl. Mater. Interfaces*, 2022, **14**, 35969–35977.
6 S. Kakumachi, T. B. Nguyen, H. Nakanotani and C. Adachi, *Chem. Eng. J.*, 2023, **471**, 144516.
7 D. E. Loy, B. E. Koene and M. E. Thompson, *Adv. Funct. Mater.*, 2002, **12**, 245–249.
8 M. S. Park and J. Y. Lee, *Chem. Mater.*, 2011, **23**, 4338–4343.
9 C. Peng, H. Liu, X. Han, F. Zhang, S. Wang and X. Li, *J. Mater. Chem. C*, 2022, **10**, 14471–14479.
10 V. G. Sree, C. Bathula, H.-K. Youi, H.-S. Kim, J. I. Sohn and H. Im, *J. Mol. Liq.*, 2021, **338**, 116708.
11 M. R. Nagar, A. Choudhury, D. Tavgeniene, R. Beresneviciute, D. Blazevicius, V. Jankauskas, K. Kumar, S. Banik, S. Ghosh, S. Grigalevicius and J.-H. Jou, *J. Mater. Chem. C*, 2022, **10**, 3593–3608.
12 K. Kutonova, B. Ebenhoch, L. G. von Reventlow, S. Heißler, L. Rothmann, S. Bräse and A. Colsmann, *J. Mater. Chem. C*, 2020, **8**, 16498–16505.
13 Q.-X. Tong, S.-L. Lai, M.-Y. Chan, K.-H. Lai, J.-X. Tang, H.-L. Kwong, C.-S. Lee and S.-T. Lee, *Chem. Mater.*, 2007, **19**, 5851–5855.
14 Z. Jiang, T. Ye, C. Yang, D. Yang, M. Zhu, C. Zhong, J. Qin and D. Ma, *Chem. Mater.*, 2011, **23**, 771–777.
15 M. Bender, K. M. Schelkle, N. Jürgensen, S. Schmid, G. Hernandez-Sosa and U. H. F. Bunz, *Macromolecules*, 2016, **49**, 2957–2961.
16 N. Nagamura, H. Sasabe, H. Sato, T. Kamata, N. Ito, S. Araki, S. Abe, Y. Sukegawa, D. Yokoyama, H. Kaji and J. Kido, *J. Mater. Chem. C*, 2022, **10**, 8694–8701.
17 X. Zhang, H. Yan, X. Zhang and H. Meng, *Sci. China Mater.*, 2024, **67**, 2767–2777.

18 K.-K. Tan, W.-L. Zhao, C.-H. Guo, W.-C. Guo, M. Li and C.-F. Chen, *Chem. Eng. J.*, 2024, **482**, 149080.
19 P. M. Borsenberger, L. Pautmeier, R. Richert and H. Bässler, *J. Chem. Phys.*, 1991, **94**, 8276–8281.
20 M. C. Suh, B. D. Chin, M.-H. Kim, T. M. Kang and S. T. Lee, *Adv. Mater.*, 2003, **15**, 1254–1258.
21 Q. Li, Z. Yu, Q. Liu, Y. Guo, Z. Fu, Y. Yang, Z. Bin, D. Wu and J. Lan, *Chem. Sci.*, 2024, **15**, 10547–10555.
22 H. Cheng, J. Lan, Y. Yang and Z. Bin, *Mater. Horiz.*, 2024, DOI: **10.1039/d4mh00634h**.
23 Y. Luo, Z. Liu, G. Yang, T. Wang, Z. Bin, J. Lan, D. Wu and J. You, *Angew. Chem., Int. Ed.*, 2021, **60**, 18852–18859.
24 Y. Tao, C. Yang and J. Qin, *Chem. Soc. Rev.*, 2011, **40**, 2943–2970.
25 X. Yang, G. Zhou and W.-Y. Wong, *Chem. Soc. Rev.*, 2015, **44**, 8484–8575.
26 S. Gangala and R. Misra, *J. Mater. Chem. A*, 2018, **6**, 18750–18765.
27 Y. Jiang, Y.-Y. Liu, X. Liu, H. Lin, K. Gao, W.-Y. Lai and W. Huang, *Chem. Soc. Rev.*, 2020, **49**, 5885–5944.
28 Y.-K. Qu, Q. Zheng, J. Fan, L.-S. Liao and Z.-Q. Jiang, *Acc. Mater. Res.*, 2021, **2**, 1261–1271.
29 Y. Chen, J. Xu and P. Gao, *Org. Chem. Front.*, 2024, **11**, 508–539.
30 Ö. Usluer, *J. Mater. Chem. C*, 2014, **2**, 8098–8104.
31 R. Braveenth, H. W. Bae, Q. P. B. Nguyen, H. M. Ko, C. H. Lee, H. J. Kim, J. H. Kwon and K. Y. Chai, *Molecules*, 2017, **22**, 464.
32 Z. Jiang, H. Yan, X. Zhang, Z. Meng, C. Kuang, X. Zhang, Y. He, Y. Zhu and H. Meng, *Adv. Opt. Mater.*, 2023, **11**, 2301014.
33 O. Usluer, S. Demic, D. A. M. Egbe, E. Birckner, C. Tozlu, A. Pivrikas, A. M. Ramil and N. S. Sariciftci, *Adv. Funct. Mater.*, 2010, **20**, 4152–4161.
34 T. P. I. Saragi, T. Spehr, A. Siebert, T. Fuhrmann-Lieker and J. Salbeck, *Chem. Rev.*, 2007, **107**, 1011–1065.
35 L. Caliò, M. Salado, S. Kazim and S. Ahmad, *Joule*, 2018, **2**, 1800–1815.
36 N. J. Jeon, H. Na, E. H. Jung, T.-Y. Yang, Y. G. Lee, G. Kim, H.-W. Shin, S. I. Seok, J. Lee and J. Seo, *Nat. Energy*, 2018, **3**, 682–689.
37 Y. Ren, Y. Wei, T. Li, Y. Mu, M. Zhang, Y. Yuan, J. Zhang and P. Wang, *Energy Environ. Sci.*, 2023, **16**, 3534–3542.
38 X. Liu, B. Ding, M. Han, Z. Yang, J. Chen, P. Shi, X. Xue, R. Ghadari, X. Zhang, R. Wang, K. Brooks, L. Tao, S. Kinge, S. Dai, J. Sheng, P. J. Dyson, M. K. Nazeeruddin and Y. Ding, *Angew. Chem., Int. Ed.*, 2023, **135**, e202304350.
39 L. Sicard, C. Quinton, J.-D. Peltier, D. Tondelier, B. Geffroy, U. Biapo, R. Métivier, O. Jeannin, J. Rault-Berthelot and C. Poriel, *Chem.–Eur. J.*, 2017, **23**, 7719–7727.
40 Y.-F. Zhang and Z.-J. Shi, *Acc. Chem. Res.*, 2019, **52**, 161–169.
41 Y. Yang, Y. Wu, Z. Bin, C. Zhang, G. Tan and J. You, *J. Am. Chem. Soc.*, 2024, **146**, 1224–1243.
42 Z. Huang, Z. Bin, R. Su, F. Yang, J. Lan and J. You, *Angew. Chem., Int. Ed.*, 2020, **59**, 9992–9996.
43 Z. Huang, B. Lei, D. Yang, D. Ma, Z. Bin and J. You, *Angew. Chem., Int. Ed.*, 2022, **61**, e202213157.
44 F. Wang, L. Zhang, W. Han, Z. Bin and J. You, *Angew. Chem., Int. Ed.*, 2022, **61**, e202205380.
45 Z. Lin, J. C. A. Oliveira, A. Scheremetjew and L. Ackermann, *J. Am. Chem. Soc.*, 2024, **146**, 228–239.
46 C. Jacob, J. Annibaletto, J. Peng, R. Bai, B. U. W. Maes, Y. Lan and G. Evano, *Angew. Chem., Int. Ed.*, 2024, **63**, e202403553.
47 J.-H. Jou, T.-H. Li, S. Kumar, C.-C. An, A. Agrawal, S.-Z. Chen, P.-H. Fang, G. Krucaite, S. Grigalevicius, J. Grazulevicius and C.-F. Sung, *Org. Electron.*, 2015, **24**, 254–262.
48 W. Jiang, X. Ban, M. Ye, Y. Sun, L. Duan and Y. Qiu, *J. Mater. Chem. C*, 2015, **3**, 243–246.
49 H. Fukagawa, T. Shimizu, H. Kawano, S. Yui, T. Shinnai, A. Iwai, K. Tsuchiya and T. Yamamoto, *J. Phys. Chem. C*, 2016, **120**, 18748–18755.
50 S. H. Jeong, H. J. Jang and J. Y. Lee, *J. Ind. Eng. Chem.*, 2019, **78**, 324–329.